Journal of Nuclear Materials 467 (2015) 848–854

Contents lists available at ScienceDirect

Journal of Nuclear Materials

journal homepage: www.elsevier.com/locate/jnucmat

Helium ion irradiation behavior of Ni-1wt.%SiC_{NP} composite and the effect of ion flux

X.L. Zhou [a, b], H.F. Huang [a, *], R. Xie [a], G.J. Thorogood [c], C. Yang [a], Z.J. Li [a], H.J. Xu [a, **]

[a] Shanghai Institute of Applied Physics, Chinese Academy of Sciences (CAS), Shanghai, 201800, China
[b] ShanghaiTech University, Shanghai, 201210, China
[c] Institute of Materials Engineering, Australian Nuclear Science and Technology Organisation, Lucas Heights, New South Wales, 2234, Australia

A R T I C L E I N F O

Article history:
Received 24 April 2015
Received in revised form
19 October 2015
Accepted 1 November 2015
Available online 10 November 2015

Keywords:
Ni-SiC_{NP} composite
Ion fluence
Ion flux
Helium bubble
Irradiation hardening

A B S T R A C T

Silicon carbide nanoparticle-reinforced nickel metal (Ni–SiC_{NP} composite) samples were bombarded by helium ions with fluences of 1×10^{16} and 3×10^{16} ions/cm^2 at two different fluxes. The microstructural and mechanical changes were characterized via TEM and nanoindentation. Nano-scaled helium bubbles in the shape of spheres were observed in the samples irradiated at high flux and polygons at low flux. The number of helium bubbles increased with the fluence, whereas their mean size remained unaffected. In addition, the nanohardness of the damage layer also increased as the fluence increased. In addition this study suggests that a higher flux results in a higher number of smaller helium bubbles, while showing no obvious effect on the irradiation-induced hardening of the materials.

1. Introduction

Molten Salt Reactors (MSR) that operate at higher temperatures than water-cooled reactors are one of the advanced Generation IV concept reactors [1,2]. The structural materials for the primary loop of MSR will be subject to extreme environments, i.e. high temperature, high neutron fluences and a corrosive coolant [3]. The Ni-based alloy, Hastelloy N was considered to be the first option for the structural metallic components in MSR due to their excellent chemical compatibility with fluoride molten salts [4]. However, Hastelloy N has limitations that hinder its application in future high-temperature MSR. The first of these is the maximum service temperature of Hastelloy N being 704 °C, this limitation will restrict the maximum allowable temperature for the coolant [5]. Secondly, helium can be produced via a two-step reaction due to the large neutron absorption cross section of Ni. This results in helium embrittlement which is a crucial issue in nuclear reactors [6]. Recently, silicon carbide nanoparticles (SiC_{NP}) have been used as a reinforcing phase for nickel metal by Huang et al. [7–9]. The research indicates that the dispersed SiC_{NP} can effectively improve the high-temperature strength of Ni-based alloy. In light of this finding, information about the helium ion irradiation damage resulting in Ni–SiC_{NP} composites is of particular importance to evaluate with respect to the application of this material in MSR. In addition, it is generally accepted that irradiation induced microstructural evolution depends on many factors, such as fluence, flux and temperatures [10–13]. It should be noted that the effect of flux is rarely reported, compared to the effects of fluence and temperature.

Hence, in this study, the Ni-1wt.%SiC_{NP} composite samples were irradiated with helium ions at the same ion fluence, whereas the ion fluxes were varied. The irradiation induced microstructural evolution and hardening were characterized via TEM and nanoindentation. The major goal of this study is to investigate the helium ion irradiation damage of Ni-1wt.%SiC_{NP} composite and to determine the relevant ion flux effect.

2. Experimental procedure

2.1. Materials and irradiation conditions

Coupons of Ni-1%wt.SiC_{NP} composite measuring $10 \times 10 \times 1$ mm^3 were cut from a bulk specimen and mechanically polished to a mirror-like finish with silicon carbide paper and diamond polishing

* Corresponding author.
** Corresponding author.
E-mail addresses: huanghefei@sinap.ac.cn (H.F. Huang), xuhongjie@sinap.ac.cn (H.J. Xu).

http://dx.doi.org/10.1016/j.jnucmat.2015.11.004
0022-3115/

paste. The surface of the coupons were then electro-polished at 36 V for approximately 10 s in an aqueous solution of 50% H_2SO_4 and 40% glycerin below 0 °C, followed by ultrasonic cleaning in acetone, alcohol and finally deionized water to ensure that mechanically induced damage was removed and the surface was clean.

Ion irradiation experiments were performed on two groups of samples detailed in Table 1. The first group were irradiated with 3 MeV He^+ ions via the ion accelerator located in Shanghai Institute of Applied Physics, Chinese Academy of Science (SINAP-CAS). The beam current density was approximately 1×10^{13} ions/(cm^2·s), and the beam was scanned both horizontally and vertically to ensure uniformity of irradiation. The samples were irradiated for 1000 and 3000 s to achieve a fluence of 1×10^{16} and 3×10^{16} ions/cm^2, corresponding to a helium concentration of 3500 and 10,500 appm, respectively. The second group of samples were irradiated with 500 KeV He^{2+} ions via the 320 KV Highly Charged Ions Research Platform of the Institute of Modern Physics, Chinese Academy of Sciences (IMP-CAS) [14]. The beam current density was approximately 2×10^{12} ions/(cm^2·s) for the second group of samples. The irradiation times were 5000 and 15,000 s respectively to achieve the same fluence as the first group of samples for a comparative purpose. All samples were kept at a constant temperature of 600 °C during irradiation via monitoring with a thermocouple with an error of ±5 °C. The damage profiles were calculated using the SRIM 2008 software package [15,16] as shown in Fig. 1, wherein the displacement energy is 40 eV [16–18]. The irradiation damage depth caused by 500 KeV and 3 MeV helium ions was approximately 1.3 and 5.3 μm, respectively, with a peak damage at depth of 0.9 and 4.9 μm respectively.

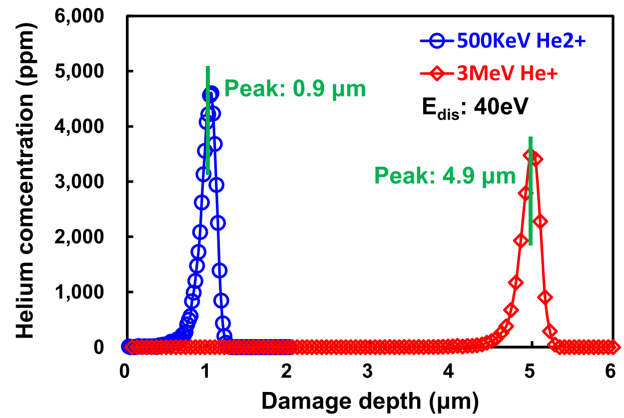

Fig. 1. Irradiation damage profile of 3 MeV and 500 KeV helium ions as a function of the depth, calculated using SRIM software.

2.2. Characterization

The ion irradiation-induced microstructural changes of the Ni-1%wt.SiC_{NP} specimens were characterized via a Tecnai G2 F20 transmission electron microscope (TEM) at an accelerating voltage of 200 kV. The specimens were prepared with a focused ion beam (FIB) mill [19,20]. The nanohardness of the unirradiated and irradiated specimens were measured with a G200 nanoindenter. A diamond Berkovich tip (model TB13989-XP) with a radius of 20 nm was employed. The experimental hardness was determined by analyzing the load–displacement (P-h) curves using the Oliver and Pharr method [21,22].

3. Results and discussion

3.1. Microstructure evolution

Fig. 2 are the bright field TEM images of sample #2. According to the damage profile calculated using SRIM, four regions (Region a–d) at different locations along the penetration track were selected to investigate the ion irradiation induced microstructural changes. Some dispersed SiC_{NP} were observed in all selected regions. The images for these four regions show clearly that no helium bubbles were identified in regions a and b, whereas a high amount of spherical helium bubbles with sizes that ranged from 3 to 6 nm were identified in region c. The presence of helium bubbles in region c was verified via through-focus experiments. In Fig. 3 for positive defocus (overfocus of the objective lens), helium bubbles appear as black dots surrounded by a white fringe while for negative defocus (underfocus), the dots are white and the fringe is dark. In region d a lower amount of similar helium bubbles were observed within an indentation depth of 5.3 μm. It should be noted that the distribution of helium bubbles along the ion penetration track are consistent with the damage profile calculated by SRIM. As for sample #1 which was irradiated at the same flux but at a lower fluence, similar observations resulted.

The microstructural changes of samples 3 and 4 were characterized with the same procedure. Unlike the case with higher flux, polygonal helium bubbles were observed in all regions, as shown in Fig. 4 (sample 4). As previously the helium bubbles were revealed using through-focus experiments. The size of the helium bubbles observed in different regions ranged from 4 to 13 nm and have no significant variations. The amount of helium bubbles in region c was the highest, however, the size and amount increased and decreased proportionally with flux. The formation of polygonal helium bubbles was also reported previously by Osamura et al. in helium ion irradiated Mo foils [23].

The implantation of high energy He ions could knock atoms in a crystal lattice from their equilibrium positions and cause collision cascades, introducing a large number of vacancies and interstitials. In this study the samples were irradiated at a temperature of up to half the materials melting temperature and some of the point defects can be annihilated by their recombination or migration to sinks. Additionally, interstitials will gather together to form dislocation loops which are always difficult to observe by TEM due to their low number, while vacancies can agglomerate into platelets or voids which can collapse into dislocation loops. In this study because of the presence of the helium atoms one possibility is that helium atoms can stabilize the small void nuclei and prevent the collapse of the void embryo into vacancy loops [24]. Helium can remain involved in the formation of voids as the nucleation process turns heterogeneous. As the concentration of the helium atoms increases, more helium participates in filling up the voids and

Table 1
Summary of the ion irradiation conditions for the Ni-1wt.%SiC_{NP} composites.

Samples no.	Type of ions	Ion energy (KeV)	Ion flux (ions/cm^2·s)	Irradiation time (s)	Ion fluence (ions/cm^2)	Irradiation temperature (°C)
#1	He^+	3000	1×10^{13}	1000	1×10^{16}	600
#2				3000	3×10^{16}	
#3	He^{2+}	500	2×10^{12}	5000	1×10^{16}	
#4				15000	3×10^{16}	